New Mexico Geological Society

Downloaded from: https://nmgs.nmt.edu/publications/guidebooks/76



New $^{40}Ar/^{39}Ar$ Age Determinations for Tomé Hill Volcano and Isleta Pueblo "Basalt Island," Central Albuquerque Basin, Rio Grande Rift: Implications for Rift Magmatism

Richard M. Chamberlin, David W. Love, and Julia Ricci
2026, pp. 193-206. https://doi.org/10.56577/FFC-76.193

in:

Geology of the Albuquerque Region - Fall Field Conference 2026, Connell, Sean D.; Koning, Daniel J.;, New Mexico Geological Society 76th Annual Fall Field Conference Guidebook, 452 p. https://doi.org/10.56577/FFC-76

This is one of many related papers that were included in the 2026 NMGS Fall Field Conference Guidebook.

Annual NMGS Fall Field Conference Guidebooks

Every fall since 1950, the New Mexico Geological Society (NMGS) has held an annual Fall Field Conference that explores some region of New Mexico (or surrounding states). Always well attended, these conferences provide a guidebook to participants. Besides detailed road logs, the guidebooks contain many well written, edited, and peer-reviewed geoscience papers. These books have set the national standard for geologic guidebooks and are an essential geologic reference for anyone working in or around New Mexico.

Free Downloads

NMGS has decided to make peer-reviewed papers from our Fall Field Conference guidebooks available for free download. This is in keeping with our mission of promoting interest, research, and cooperation regarding geology in New Mexico. However, guidebook sales represent a significant proportion of our operating budget. Therefore, only *research papers* are available for download. *Road logs*, *mini-papers*, and other selected content are available only in print for recent guidebooks.

Copyright Information

Publications of the New Mexico Geological Society, printed and electronic, are protected by the copyright laws of the United States. No material from the NMGS website, or printed and electronic publications, may be reprinted or redistributed without NMGS permission. Contact us for permission to reprint portions of any of our publications.

One printed copy of any materials from the NMGS website or our print and electronic publications may be made for individual use without our permission. Teachers and students may make unlimited copies for educational use. Any other use of these materials requires explicit permission.

This page is intentionally left blank to maintain order of facing pages.

New Mexico Geological Society Guidebook, 76th Fall Field Conference, 2026, p. 193–205, https://doi.org/10.56577/FFC-76.193

NEW ^{40}AR/^{39}AR AGE DETERMINATIONS FOR TOMÉ HILL VOLCANO AND ISLETA PUEBLO "BASALT ISLAND," CENTRAL ALBUQUERQUE BASIN, RIO GRANDE RIFT: IMPLICATIONS FOR RIFT MAGMATISM

RICHARD M. CHAMBERLIN[1], DAVID W. LOVE[1], AND JULIA RICCI[2]

[1]New Mexico Bureau of Geology and Mineral Resources, 801 Leroy Pl., Socorro, NM 87801 (emeritus); Richard.Chamberlin@nmt.edu
[2]New Mexico Bureau of Geology and Mineral Resources, 801 Leroy Pl., Socorro, NM 87801

Abstract—This paper presents new ^{40}Ar/^{39}Ar age determinations for the dacitic Tomé Hill volcano and the river-level "basalt island" at Isleta Pueblo. Lavas from the Tomé Hill volcano yield a mean age of 3.813 ± 0.043 Ma (n = 2), indistinguishable from a published mean age of 3.83 ± 0.05 Ma (n = 3) for dacitic lava at the "SW edifice", south of the Los Lunas volcano. The eruptive center at the SW Edifice is spatially distinct; it is renamed here the "Dalies volcano." Tomé and Dalies lavas are chemically very similar, have a common mineralogy, contain granitoid xenoliths, exhibit reverse-zoned plagioclase, and have elevated ^{87}Sr/^{86}Sr ratios. These observations imply hybrid magma evolution involving assimilation and fractional crystallization in an open magma system. Although 10 km apart, the Tomé and Dalies volcanoes were coeval and likely had a common magma source. Residual basaltic melt, of ~23 km^3, remaining in the lower crust after eruption of the nearby Wind Mesa shield volcano (4.06 ± 0.16 Ma, 5.7 km^3) is likely to have been the initial melt source for the Tomé–Dalies system. The previously undated river-level "basalt island" at Isleta Pueblo yields a precise ^{40}Ar/^{39}Ar age of 2.794 ± 0.015 Ma. New and published data define two geochemically and stratigraphically distinct lavas at Isleta: (1) a MgO-rich (6.3–8.3 wt% MgO) lower basalt flow at the river-level "basalt island" and (2) a relatively potash-rich (1.5–1.7% K_2O) upper trachybasalt that forms most of the Isleta volcano. River-level lavas are assigned to the Isleta Pueblo volcano. The latter yield a weighted mean age of 2.81 ± 0.01 Ma (n = 5), indistinguishable from a weighted mean age of 2.81 ± 0.02 Ma (n = 4) for the stratigraphically younger Isleta volcano. A cross-section allows at least 7 m of sediment accumulation between the two eruptions. Overall, the Isleta complex appears to record an open magma system in which rapid alkali enrichment (volatile related) was followed relatively quickly by a new pulse of basaltic magma into the same crustal reservoir. Nine basaltic eruptions have occurred in the Isleta region between about 4 and 0.1 Ma. This cluster of nine volcanoes is co-located with a seismic velocity anomaly in the underlying crust where the shear-wave propagation velocity (dVs) is 3–5% faster. We interpret this anomaly as representing gabbroic basement that acts an efficient and refractory (i.e., hard-to-melt) "mafic magma pipeline" (MaMagPi) for transport of high-temperature basaltic magma, via dikes, to the surface of the rift basin near Isleta.

INTRODUCTION

A Cluster of Volcanoes

This paper presents three new ^{40}Ar/^{39}Ar age determinations, two for the dacitic Tomé Hill volcano and one for the "basalt island" that forms the bedrock foundation at Isleta Pueblo (Table 1). These volcanic features have not been previously dated by the ^{40}Ar/^{39}Ar method. The Tomé Hill volcano was previously dated by the imprecise K–Ar method to 3.4 ± 0.4 Ma (Bachman and Mehnert, 1978). Lavas from the highly eroded Tomé Hill volcano yield a new mean age of 3.813 ± 0.043 Ma (n = 2). The "basalt island" at Isleta Pueblo yields a precise age determination of 2.794 ± 0.015 Ma. Relatively MgO-rich basalt lavas at Isleta Pueblo, including the "basalt island" (Fig. 1), occur immediately adjacent to the Holocene floodplain of the Rio Grande. These MgO-rich exposures are referred to here as "river-level" basalt lavas in order to distinguish them from the stratigraphically younger trachybasalt lava that forms the topographically higher Isleta volcano.

TABLE 1. Summary of new ^{40}Ar/^{39}Ar ages for the Isleta Pueblo "basalt island" and Tomé Hill volcano.

Samples	Rock type	Unit	Lat. (°N)	Lon. (°W)	Material	Plateau (Ma)	±2σ	N	% ^{39}Ar	MSWD
DL-ISP-1	Basalt	Isleta Pueblo*	34.90857	106.69697	Groundmass	**2.794**	**0.015**	6/13	58.2	1.0
TH-1	Dacite	Tomé-SE	34.75199	106.70403	Groundmass	3.786	0.029	3/13	51.7	2.8
TH-2	Dacite	Tomé-NW	34.75862	106.71029	Groundmass	3.830	0.023	6/14	81.2	2.0
					TH-weighted mean:	**3.813**	**0.043**			

Method was resistance furnace incremental heating of groundmass concentrates. Ages calculated relative to Fish Canyon Tuff monitor with a value of 28.201 ± 0.023 Ma (Kuiper et al., 2008) and the total 40K decay constant 5.463 × 10^{-10}/a of Min et al. (2010). MSWD = mean square of weighted deviates; N = number of steps used for the plateau age calculation. Bold font indicates the preferred ages. Samples: DL-ISP-1 collected by D. Love; TH-1 and TH-2 collected by R. Chamberlin. *Correlates to the Isleta Pueblo "basalt island" referred to in text. Locations are in decimal degrees and NAD 83 datum.

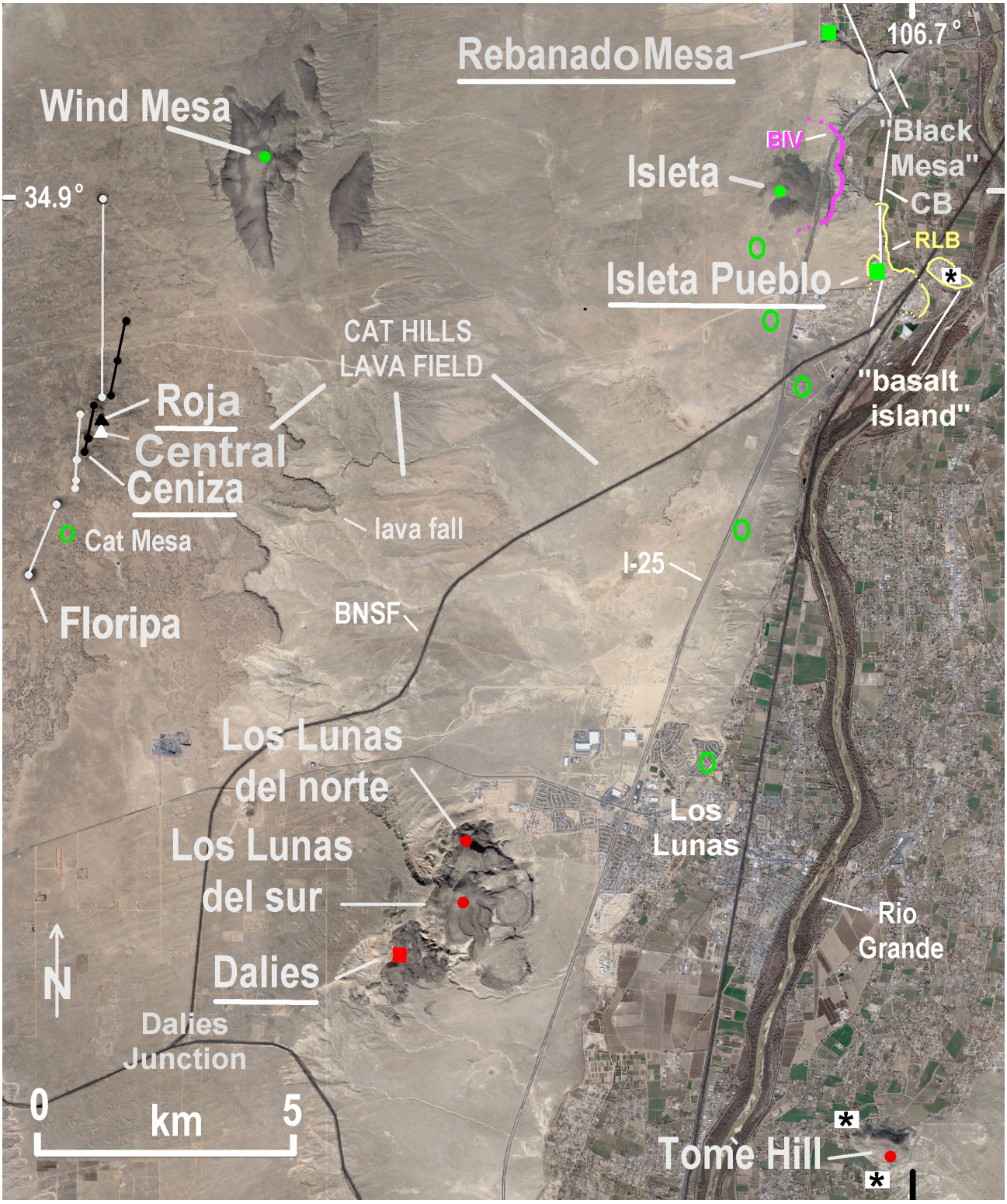


FIGURE 1. Map of Pliocene to Pleistocene eruptive centers (volcanoes) in the Los Lunas volcanic cluster (LLVC). Vent locations for individual basaltic volcanoes near Isleta are indicated by green dots. In the basaltic Cat Hills, older tephra cones (black dots) and younger tephra cones (white dots) are aligned along two distinct fissure trends. Published age determinations indicate four episodes of eruption in the Cat Hills field (Table 2). Each of the dated vent locations (cones) has been given an informal name of convenience: from oldest to youngest, Roja (black triangle), Ceniza (black dots), Floripa (white dots), and Central (white triangle). Two topographic levels of basaltic flows are present at Isleta. The older "river-level basalt" (RLB, yellow line) occurs just above the Holocene floodplain. The eastern base of the Isleta volcano (BIV, magenta line) is well exposed about 30 m above the floodplain. Vent locations for andesite and dacite volcanoes are denoted by red dots. Green circles represent aeromagnetic anomalies interpreted as shallow buried intrusions (Grauch and Connell, 2013, appendix G2). Newly recognized volcanic vents (Figs. 3A–3D) are shown with green or red squares. New and published ages of eruptive centers are listed in Tables 1 and 2. New names of convenience are underlined. Asterisks show sample locations for this report. "Black Mesa" is now well dated (Table 2), and its eroded vent has been located (Fig. 3A); it is here informally renamed "Rebanado Mesa" (Fig. 3B). CB = Coors Boulevard. *Base image is from Google Earth, © 2010 Landsat / Copernicus.*

Here, we synthesize these new age data with published age and compositional data for Pliocene to Pleistocene eruptive centers in the Isleta–Los Lunas area. The goal is to develop a local volcanic history that may in turn reflect upon the character and "plumbing" of the relatively young magma system under this central portion of the Albuquerque Basin and the Rio Grande rift.

Three well-known volcanic landforms are commonly recognized as forming a cluster of basaltic volcanoes near Isleta. These include the broad, gentle slopes of the Wind Mesa shield volcano; the prominent Isleta volcano, next to Interstate 25; and the numerous small black cinder cones of the Cat Hills west of I-25 (Kelly and Kudo, 1978). The aligned cinder cones that form the Cat Hills mark two different fissure systems that fed the broad expanse of the Cat Hills lava field. About 10 km south of Isleta, the volcanic landforms are different in morphology and composition. West of Los Lunas, chocolate-brown andesite lava forms a thick pile of stubby, overlapping flows that comprise the Los Lunas volcano. Southeast of Los Lunas, Tomé Hill is the eroded remnant of what was originally a much larger volcano of dacitic composition, once probably similar in size and shape to the younger Los Lunas volcano.

This tight grouping of Pliocene and Pleistocene volcanoes between Wind Mesa and Tomé Hill is referred to here as the Los Lunas volcanic cluster (LLVC). The coeval Albuquerque volcanoes, 25 km north of Isleta, could be included in the LLVC; for brevity, however, they are omitted from this study. Figure 1 is a map of the 13 eruptive centers that comprise the LLVC. For this report, an "eruptive center" is a volcano that may or may not (e.g., Tomé Hill) have the typical landform of a volcano. In other words, as used here the terms "eruptive center" and "volcano" are synonymous and may be interchanged. Also, a suite of fissure-fed (aligned) tephra cones formed by one well-dated eruption, such as the Albuquerque volcanoes (Zimmerer, 2024), is here considered to be a single "eruptive center."

Figure 1 is based primarily on all available $^{40}Ar/^{39}Ar$ ages, along with vent locations and vent morphology obtained by interpretation of Google Earth images (see Appendix Tables 1, 2, and 3). Previously published age determinations, relevant to the LLVC, are combined in Table 2 with the new data from this report. The combined datasets provide a new overview of the local eruptive sequence and periods of repose. All age data reported here are based on the presently accepted Fish Canyon Tuff monitor age (FCT-2) of 28.201 Ma. Figure 2 shows a panorama of eight basaltic volcanoes that comprise the northern sector of the LLVC. Not visible in the panorama is the well-dated 3.1-My-old Cat Mesa basaltic volcano, whose vent is buried under the Cat Hills (Kelly and Kudo, 1978). Geomorphic analysis using Google Earth images has been a significant resource in identifying previously unknown vent locations (Fig. 3) for several LLVC eruptive centers (that is, volcanoes).

A notable aspect of Figure 1 is that basaltic volcanoes (green dots, plus white and black dots of Cat Hills tephra cones) form a northern subcluster of nine well-dated eruptive centers (Table 2), whereas four andesitic volcanoes (red dots) form a coeval southern subcluster at Tomé Hill, Dalies, and the two overlapping lava piles at Los Lunas volcano (Love et al., 1998). This compositional pattern of relatively young volcanoes may reflect compositional differences in the underlying crystalline basement rocks of Proterozoic age that constitute more than 90% of the crustal section. Golos et al. (2020) have published seismic velocity maps of the continental United States that show variations in primary-wave propagation velocity (dVp) and shear-wave propagation velocity (dVs) along horizontal slices at 20 km, 40 km, and down to 200 km depth. In the central Albuquerque Basin, their maps show a small (~20 x 40-km) velocity anomaly east of 107° W and mostly south of 35 °N, which includes the Wind Mesa, Isleta, and Cat Hills area. In this anomaly, the dVs is about 4–5% faster at 20 km and 2–3% faster at 40 km depth, while the dVp is about 1–2% faster at 20 km and 2–3% faster at 40 km depth. In comparison, the area of the Socorro Magma Body shows dVs about 1–2% slower at 20 km depth and 4–5% slower below the magma body at 40 km depth. We interpret the shear-wave velocity anomaly beneath Isleta as reflecting relatively dense (e.g., 2.8–3.0 Mt/m^3) mafic crystalline basement rocks, such as gabbro and metabasalt, that are also more refractory (i.e., have a higher melting temperature) than the surrounding basement rocks, which are predominantly of granitic composition (Condie and Budding, 1979).

Many earth scientists now subscribe to the emerging paradigm that crustal magma reservoirs (sills) grow and evolve by incremental additions of relatively small batches of basaltic melt that are squeezed, by ductile shear, from the melt-saturated (<0.5% melt) upper asthenosphere (Katz et al., 2006; Annen, 2011; Cashman et al, 2017; Debayle et al., 2020).

TABLE 2. Published and new $^{40}Ar/^{39}Ar$ ages for the LLVC.

Eruptive center	Age (Ma)	±2σ	Reference
Cat Hills cones and lava field (four eruptive centers)			
Central dike (n = 2)	0.1155	0.0056	Z
Floripa cones (n = 4)	0.1466	0.0010	Z
Ceniza cones (n = 1)	0.2681	0.0013	Z
Roja cone (n = 1)	0.496	0.160	M
Los Lunas volcano (two eruptive centers)			
Del Sur vent (n = 7)	1.271	0.014	D
Del Norte vent (n = 1)	1.31	0.05	D
Rebanado Mesa volcano (n = 1)	2.71	0.04	M
Isleta volcanic complex (two eruptive centers)			
Isleta volcano (n = 4)	2.81	0.02	Table 3
Isleta Pueblo volcano (n = 5)	***2.81***	***0.01***	***Table 3***
Cat Mesa volcano (n = 1)	3.04	0.10	M
Tomé–Dalies system (two coeval volcanoes, one reservoir)			
Tomé Hill volcano (n = 2)	***3.813***	***0.043***	***TR***
Dalies volcano (n = 3)	3.83	0.05	D
Wind Mesa volcano (n = 1)	4.06	0.16	M

New $^{40}Ar/^{39}Ar$ ages are shown in bold italics. References: Z, Zimmerer (2024); M, Maldonado et al. (2007); D, Dunbar et al. (2016); C, Connell et al. (2013); TR, this report. Connell et al. (2013) redated splits from the same sites as Maldonado et al. (2007). See Tables 1 and 3 for details of new age determinations and recalculated ages of the Isleta complex.

Relatively little extensional tectonic force is needed to initiate rapid transport of buoyant batches of basaltic magma through the lithospheric mantle and crust via magma-driven hydraulic fractures, also known as dikes (Buck, 2004). This suggests that the Rio Grande rift is not pulling apart by mechanical stretching; rather, the lithosphere is being driven apart by magmatic splitting. Another important consideration is that volcanic eruptions generally represent less than 20% of the volume of the original source reservoir (White et al., 2006). In other words, slightly more than 80% of the magma remains in the source reservoir after an eruption. With this perspective, the focus here is on how the new age constraints on Tomé Hill and the Isleta Pueblo "basalt island" might be linked to incremental magma intrusion and related residual magmas under the Isleta–Los Lunas region.

Previous Age Dating

In their now-classic work, Kelly and Kudo (1978) presented comprehensive geologic descriptions, detailed geologic maps, whole-rock chemical analyses, and petrographic data for the Isleta, Wind Mesa, Cat Hills, Los Lunas, and Tomé Hill volcanoes. The K–Ar ages they reported for Isleta (2.78 ± 0.12 Ma) and the Cat Hills (0.140 ± 0.038 Ma) are remarkably consistent with more recently published $^{40}Ar/^{39}Ar$ ages (Table 2). Access to the basaltic volcanoes on Isleta Pueblo lands is now generally restricted, and thus the work of Kelly and Kudo (1978) remains a foundational reference for future geologic studies in the area. As they described, the presence of glomerocrysts, ultramafic inclusions, and coarse plagioclase phenocrysts at Wind Mesa, Isleta, and Cat Mesa, respectively, are all suggestive of extended residence time and crystallization in the lower crust, followed by disruption of the magma reservoirs.

Maldonado et al. (2007) published a geologic map of the Pueblo of Isleta tribal lands as part of a U.S. Geological Survey study of groundwater resources in the area. Much of the volcanic geology described by Kelly and Kudo (1978) was incorporated into this broader study. Table 1 of Maldonado et al. (2007) summarizes several $^{40}Ar/^{39}Ar$ ages for Cat Hills, Black Mesa, Isleta (main edifice), a river-level lava east of the Isleta volcano, Cat Mesa, and Wind Mesa. These authors reported ages that include 100 ± 20 ka, 113 ± 30 ka, 253 ± 80 ka, and 496 ± 160 ka for lavas of the Cat Hills lava field. They noted that the two older ages were stratigraphically inconsistent with the map relationships of Kelly and Kudo (1978), and they interpreted the Cat Hills lava field as the product of a monogenetic eruption between 100 ka and 113 ka.

Geomorphic analysis of Cat Hills tephra cones, coupled with published geochemical data (see Appendix Table 3, as well as Figs. 1 and 2), shows two morphologically and geochemically distinct suites of tephra cones: (1) younger cones (white dots in Fig. 1) characterized by well-preserved central depressions (craters) and associated with relatively high MgO (6.7–8.2 wt%) basaltic lavas and (2) older cones (~253 ka; black dots in Fig. 1) that lack central depressions and stand 30–60 m higher in elevation than the younger cones. The older cones are associated with more evolved trachybasalt lavas (5.4–6.4 wt% MgO). These observations, together with new age determinations from Zimmerer (2024; see below), support the interpretation that two or more eruptive episodes occurred within the Cat Hills lava field. Notably, the more evolved magma erupted first.

Four basalt samples have been collected at and near the Isleta volcano (Fig. 1) for three different projects. Maldonado et al. (2007, table 1) dated two lava samples from the main edifice (samples 19 and 20), one river-level lava (sample 18) and one xenolithic lava block from the tuff breccia that underlies the main volcanic edifice (sample 21). Splits of four of these samples were redated and relabeled by Connell et al. (2013, table 2), but to maintain sample-label continuity we will refer to these newer samples respectively as S18, S19, S20, and S21 (based on notes in the comments field of table 2 of Connell et al., 2013). Splits of the same four samples (DL-18, DL-19, DL-20, and DL-21) were collected for XRF analysis by Dave Love (this study). Note that in our manuscript the numerical suffix indicates the same sample, whereas the prefix identifies the three aforementioned studies.

Age data from the two earlier studies of the Isleta volcanic complex (Maldonado et al., 2007; Connell et al., 2013), plus the new age of the "basalt island" (Table 1), are summarized in Tables 2 and 3. Considering analytical uncertainties, each sample and its split yield indistinguishable ages. Because they represent the same, or equivalent, material, their average is the most representative age. The original sample 21 was collected

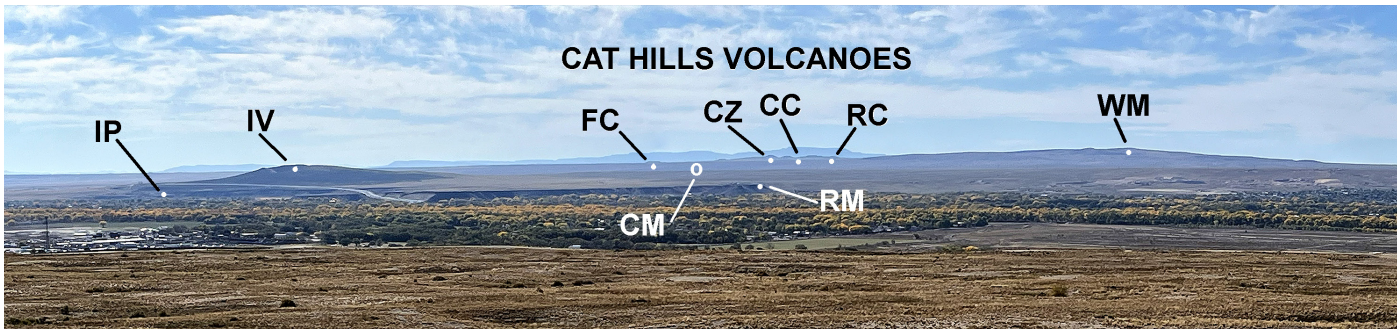


FIGURE 2. Looking west across the Isleta–Wind Mesa area. Basaltic eruptive centers are indicated by white dots just below the topographic vent. The white circle indicates the buried vent for the Cat Mesa volcano (CM). The gentle south slope of the Wind Mesa shield volcano is 2 km long. WM = Wind Mesa volcano; RM = Rebanado Mesa volcano; IV = Isleta volcano; IP = Isleta Pueblo volcano. Dated vents of the Cat Hills field, from oldest to youngest: RC = Roja cone; CZ = Ceniza cone; FC = Floripa cone; CC = Central dike 1. Photograph taken from Mesa del Sol by R. Chamberlin and enhanced by D. Love.

along the east side of I-25 (34.91734° N, −106.71989° W) from a xenolithic block of basalt chemically similar to the "river-level" basalt at Coors Road and the "basalt island." The ages of samples 21 and S21 are therefore averaged into the "river-level" basalt lavas of the Isleta Pueblo volcano. Table 3 shows that the weighted mean ages of the Isleta volcano and river-level Isleta Pueblo volcano are indistinguishable.

Two well-dated episodes of eruption are now recognized in the vicinity of the Los Lunas volcano (Dunbar et al., 2016). The andesitic main edifice of the Los Lunas volcano yields a mean $^{40}Ar/^{39}Ar$ age of 1.271 ± 0.014 Ma, n = 7, and a small exposure of dacitic lava to the south, called the "SW edifice," yields a mean age of 3.83 ± 0.05 Ma, n = 3 (Dunbar et al., 2016). Because the "SW edifice" is spatially and compositionally distinct, we refer to it in this report as the "Dalies volcano," for the well-known railroad junction about 5 km to the west. Geologic mapping of the andesitic Los Lunas volcano shows two overlapping lava piles locally separated by several meters of eolian sand (Love et al., 1998, 2001). A single sample from what is mapped as the older lava pile (Qlv1) yields an age of 1.31 ± 0.05 Ma (Dunbar et al., 2016; Table 2).

Zimmerer (2024) applied ultra-high-precision $^{40}Ar/^{39}Ar$ dating of latest Pleistocene to Holocene volcanic fields to evaluate volcanic hazards across New Mexico, including along the Jemez lineament and the Rio Grande rift. Zimmerer identified three pulses of eruptions from seven high-precision age determinations of the Cat Hills lava field, at 115.5 ± 5.6 ka (central cone, Fig. 2), 145.6 ± 10.0 ka (Floripa cone, Fig. 2), and 268.1 ± 10.3 ka (Ceniza cone, Fig. 2). A fourth pulse of eruption at the beveled Roja cone is supported by an age of 0.496 ± 0.16 Ma from lava southeast of the red cone (Maldonado et al., 2007). Although less precise, this age is distinctly older than that of the Ceniza cone (Table 2).

The morphology of the Cat Hills lava field (Fig. 1) is in agreement with the new age data of Zimmerer (2024). The Cat Hills lavas lie at two distinct levels in the landscape. A "frozen" lava fall (Fig. 1) separates the younger pulse of Floripa lavas, at the eastern end of the lava field, from the older Ceniza lavas surrounding the highest cones near the center of the lava field (Kelly and Kudo, 1978; Figure 17, Qb4).

Geologic Setting of the LLVC

Except for the late Pleistocene Cat Hills lava field, all volcanoes of the Los Lunas volcanic cluster (LLVC) erupted into the subsiding Belen sub-basin during the aggradation of Upper Santa Fe Group beds deposited by two southerly flowing river systems (Connell et al., 2013). Deposits of the south-southeasterly flowing ancestral Rio Puerco system are now assigned to the Ceja Formation (Connell, 2008), whereas deposits of the southerly flowing ancestral Rio Grande, together with intertonguing piedmont deposits, are assigned to the Sierra Ladrones Formation (Connell et al., 2001; Connell, 2004). The influence of "suddenly appearing" volcanic highlands on depositional facies of contemporaneous river systems is essentially unknown. There is, however, some evidence for the erosive powers of river systems on volcanic highlands. The steep-sided

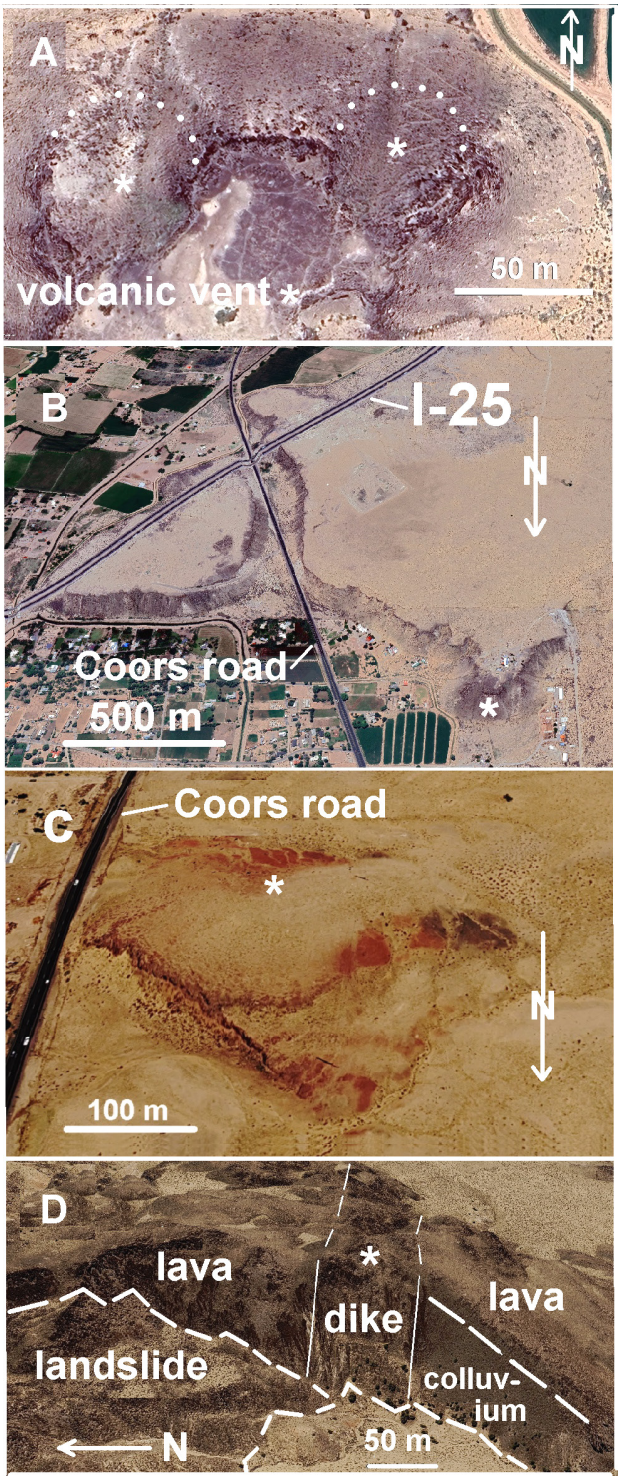


FIGURE 3. Google Earth images showing the morphology of newly recognized volcanic vents (asterisks), which are eroded remnants of Pliocene volcanoes. A) (34.9499 °N, 106.7174 °W) Map view of two deeply eroded tephra cones at the northwest terminus of Rebanado Mesa (new name; aka. Black Mesa). Dotted lines illustrate the arcuate eroded portion of the tephra cones; the dark line between the arcs may be the top of a dike that acted as a buttress, resisting erosion. B) Aerial oblique view of Rebanado Mesa looking south, showing the vent and an antecedent river canyon that sliced the mesa in half in late Pleistocene time. C) (34.9098 °N, 106.7075 °W) Aerial oblique view, looking south at red cinders in the eroded vent structure for the Isleta Pueblo volcano, source of the "basalt island" at Isleta. D) (34.7883 °N, 106.8091 °W) Oblique view, looking east, showing the feeder dike for the deeply eroded Dalies volcano.

Los Lunas lava domes (~1.31–1.27 Ma) erupted into a southerly or southeasterly flowing river system near the time of maximum aggradation of the Santa Fe Group. Thus, significant erosion and landslides on the north flank of the Los Lunas volcano may be attributed to the erosive powers of either the ancestral Rio Puerco or the ancestral Rio Grande. In contrast, the fluvial erosion and truncation of the Rebanado Mesa volcanic vent plus sculpting of the Isleta Pueblo vent (Figs. 3A–3C) are attributed to exhumation of the Pliocene volcanoes and then downcutting of the Rio Grande in late Pleistocene time.

Grauch and Connell (2013) present a new perspective on the structure of the Albuquerque Basin using a geophysical model based on a significant density contrast between upper Cenozoic sedimentary units of the Santa Fe Group and underlying Mesozoic to pre-Mesozoic rocks. In Appendix G of their comprehensive model, Grauch and Connell discuss new insights and uncertainties related to their model in the vicinity of the Los Lunas volcanic cluster. Figure G2 of the appendix to their paper shows a gravity-guided isopach map of the Santa Fe Group and surface exposures of volcanic rocks in the LLVC. This isopach map also shows the subsurface extent of buried volcanic rocks, at depths of less than 250 m, using high-resolution aeromagnetic data.

Notably, buried volcanic rocks are apparently present as far as 4 km north of the vent for the Wind Mesa shield volcano and 11 km to the south of the Wind Mesa volcano. The aeromagnetic map also shows four tongues of lava extending from 5 to 10 km to the south and southeast of the Isleta volcanic center.

TABLE 3. Original, repeat, and new $^{40}Ar/^{39}Ar$ age determinations for the Isleta volcanic complex.

Sample	Age (Ma)	±2σ	Ref.	Comments
Isleta volcano (main edifice, trachybasalt)				
19	2.82	0.06	M	I-25 SE, above 21
125S (S19)	2.89	0.07	C	Repeat date of 19
20	2.79	0.03	M	I-25 NW, basal flow
IV1 (S20)	2.82	0.03	C	Repeat date of 20
Isleta volcano, mean age: 2.83 ± 0.04 Ma (n = 4)				
Weighted mean age: 2.81 ± 0.02 Ma (n = 4)				
Isleta Pueblo volcano (river-level olivine basalt)				
21	2.83	0.04	M	Xenolith in Isleta tuff
225 (S21)	2.86	0.03	C	Repeat date of 21
18	2.77	0.04	M	Coors Road
85 (S18)	2.84	0.05	C	Repeat date of 18
DL-ISP-1	2.794	0.015	TR	Basalt island
Isleta Pueblo volcano, mean age: 2.81 ± 0.03 Ma (n = 5)				
Weighted mean age: 2.81 ± 0.01 Ma (n = 5)				

References: M, Maldonado et al. (2007); C, Connell et al., 2013); TR, this report. Connell et al. (2013) redated splits of samples from Maldonado et al. (2007). Ages are calculated with FCT monitor age of 28.201 Ma. Original and repeat ages are indistinguishable. Averages of duplicated ages are accepted as preferred mean ages as shown in Table 2. Preferred ages (weighted means) are shown in bold font. S18, S19, S20, and S21 indicate samples are splits from the original samples of Maldonado et al. (2007) (Connell et al., 2013, table 2, comments).

Altogether, the surface area of the LLVC would be about twice as great if the Pliocene volcanic rocks were not partly buried by the upper Santa Fe Group.

METHODS AND RESULTS

Sample Collection

Two lava samples from Tomé Hill were collected during a reconnaissance of the volcanic highland, guided by the geologic map of Kasten (1977). Sample TH-1 was collected near the road on the southeast flank of the hill from a colluvial block situated below a narrow, west-dipping ledge of vaguely flow-banded lava. Kasten (1977) mapped this narrow ledge as an intrusion; however, it may alternatively represent a toreva-type landslide block. A sledge was used to break the block and collect a fresh sample from its core. Sample TH-2 was collected on the northwestern flank of Tomé Hill, near the maintenance road for an irrigation canal and below horizontal cliff-forming lava flows. The sample was taken from a colluvial block about 40 m below the cliff. The block was broken with a sledge and a fresh 2-kg sample collected from its core.

A sample of lava from the "basalt island" at the Isleta Pueblo (DL-ISP-1) was collected during geologic mapping of the Isleta 7.5-minute quadrangle. The relatively fresh, non-vesicular sample was obtained from a waste pile adjacent to a recently excavated irrigation ditch. The geologic map of Maldonado et al. (2007) shows the location and geometry of the "basalt island" relative to the same river-level basalt exposure at Coors Road. A late Pleistocene to Holocene river-channel deposit separates the lava island from the exposures along Coors Road (Fig. 1).

Petrography

Standard thin sections of the above samples were examined using a Zeiss petrographic microscope. Sample TH-1 is a light gray, vaguely trachytic, sparsely porphyritic dacite with about 2–4% fine-grained plagioclase phenocrysts (1–1.5 mm) and 1–2% fine needles of partially to completely oxidized hornblende in a milky, light-gray cryptocrystalline matrix. Cores of some larger euhedral plagioclase crystals display sieve textures with unaltered continuous rims. Some unaltered cores of hornblende have optical properties of orthopyroxene, suggesting that the hornblende is replacing pyroxene in the melt due to addition of volatiles. Sample TH-2 is a porphyritic dacite very similar to TH-1. Plagioclase phenocrysts are slightly larger, as much as 2.5 mm, and somewhat more abundant (3–5%). Again, hornblende needles are variably oxidized, and larger plagioclase phenocrysts have resorbed cores with sieve textures.

Sample DL-ISP-1 is a dark-gray, fine-grained basalt with 5–7% fine-grained (1.5–1.8-mm), reddish-brown (hydrated) olivine phenocrysts and 2–3% fine-grained plagioclase phenocrysts (1.5–2 mm). Plagioclase displays a seriate texture from 0.1 to 2 mm. The microcrystalline groundmass consists predominantly of clinopyroxene, with 5–10% iron oxides and

seriate plagioclase. Euhedral olivine phenocrysts are variably altered (50–100%) to iddingsite. About one-third of olivine occurs in glomerophyric aggregates as much as 4 mm across. Less common, gabbro-like masses of plagioclase, olivine, and minor pyroxene are as much as 5 mm across. Olivine tends to be unaltered in the crystal aggregates. Crystal aggregates form about 2–4% of the rock.

Argon Geochronology

Groundmass from the three samples (TH-1, TH-2, and DL-ISP-1) was concentrated using standard mineral separation techniques. Initially, the crushed samples were sieved to a size range of 350—600 μm to expose phenocrysts, which could contain excess argon. The samples were then treated with dilute nitric acid (HNO_3) in an ultrasonic bath for 10–15 min to remove any secondary clays or carbonate grains and rinsed three times with deionized water. Groundmass grains were carefully handpicked under a binocular microscope to select fragments free of phenocrysts, ensuring the isolation of uncontaminated material for accurate dating analyses.

To perform the $^{40}Ar/^{39}Ar$ analyses, the samples were irradiated for 2 hours at the Oregon State TRIGA nuclear research reactor (Corvallis, Oregon). The Fish Canyon tuff sanidine standard with an assigned age of 28.201 ± 0.023 Ma (Kuiper et al., 2008) was used as the neutron flux monitor. The J-value (a factor to normalize variable neutron flux) for each sample was determined using a combination of eight single-grain laser fusion analyses measured at eight radial positions around the irradiation disc. Correction factors for interfering neutron reactions were determined using co-irradiated CaF_2 and K-glass (K-doped man-made glass). The total decay constant of 5.463 x 10^{-10}/a (Min et al., 2000) and the $^{40}Ar/^{36}Ar$ atmospheric ratio of 295.5 ± 0.5 (Nier, 1950) were used for age calculations. The samples were analyzed by the incremental step-heating method using a defocused diode laser to heat the samples, and argon isotopes were measured using a ThermoFisher Scientific Helix MC multi-collector mass spectrometer. Data reduction and age calculation were performed using Pychron Software (Fig. 4, Table 1; Ross, 2019). All uncertainties are reported at the 2σ confidence level. $^{40}Ar/^{39}Ar$ ages and related information are summarized in Table 1 $^{40}Ar/^{39}Ar$ results are shown as release spectra in Figure 4.

All samples exhibit a generally flat spectrum with well-defined plateau age, characterized by at least three contiguous steps overlapping within 2σ uncertainty and comprising at least 50% of the total ^{39}Ar released (e.g., McDougall and Harrison, 1999). The associated mean square of weighted deviates (MSWD) values ranges from 1.0 to 2.8, indicating statistically normal distribution at the 95% confidence level (Mahon, 1996; Table 2, Fig. 4)

In detail, sample TH-1 from Tomé Hill yields a well-defined plateau age of 3.786 ± 0.029 Ma (MSWD = 2.8; Fig. 4A). The increase in apparent age at higher temperature, consistent with excess argon, is likely associated with a high-temperature degassing phase, such as plagioclase. Sample TH-2, from the northeast flank of Tomé Hill, displays a well-defined plateau age of 3.830 ± 0.023 Ma (MSWD = 2.0; Fig. 4B). Within analytical uncertainties, ages obtained for TH-1 and TH-2 are indistinguishable. Sample DL-ISP-1, from the "basalt island"

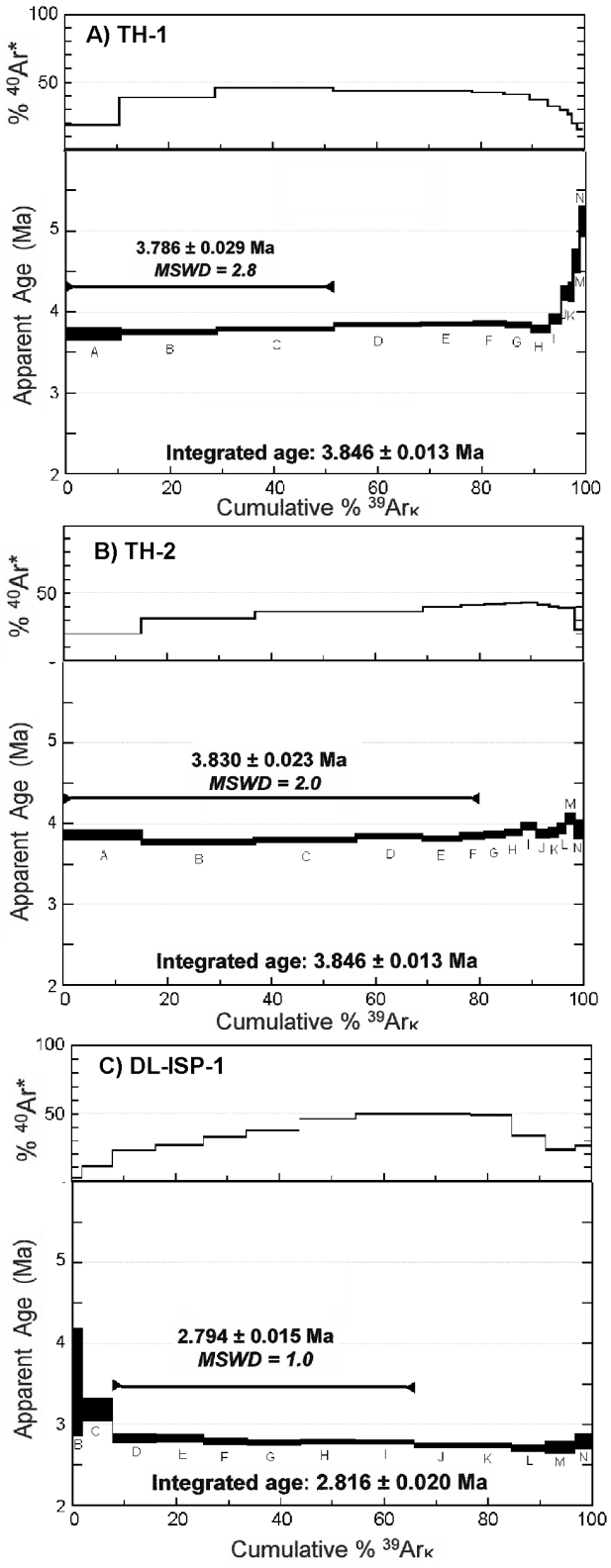


FIGURE 4. $^{40}Ar/^{39}Ar$ step-heating spectra and radiogenic yield diagrams for groundmass separates of samples collected at Tomé Hill (A and B), plus the "basalt island" at Isleta Pueblo (C). See Table 1 for details and sample locations.

at Isleta Pueblo, exhibits an overall flat spectrum, with minor excess argon present in the lowest-temperature steps. The plateau age, defined by about 58% of the released ^{39}Ar, is 2.794 ± 0.015 Ma (MSWD = 1.0; Fig. 4C).

Whole-rock Geochemistry

Splits of the three samples (TH-1, TH-2, and DL-ISP-1) were submitted to the Hooper Geoanalytical Laboratory (Pullman, Washington) for whole-rock X-ray fluorescence (XRF) and inductively coupled plasma mass spectrometry (ICP-MS) analyses. The Hooper laboratory employs low-dilution lithium tetraborate–fused beads for XRF analysis (a detailed description of their analytical methods is available online at pdxschlor.library.pdx edu. viewcontent). An additional four samples from the Isleta basalts (DL-18—DL-21) were analyzed at the New Mexico Bureau of Geology and Mineral Resources (NMBGMR) XRF laboratory using standard methods (described in Appendix 5 of Chamberlin et al., 2004, at https://geoinfo.nmt.edu/publications/monographs/bulletins/160/). The results of both analyses are summarized in Table 4, along with data from the Dalies volcano (or "SW edifice") for comparison (Dunbar et al., 2016, table 1). The geochemical classifications of lavas from the Tomé Hill, Dalies, Isleta, and Isleta Pueblo volcanoes are shown in the abbreviated total alkali–silica (TAS) diagram in Figure 5. Lavas from Tomé Hill and Dalies form a tight compositional cluster near the dacite–andesite/trachyandesite boundary. The stratigraphically older basalt of the Isleta Pueblo volcano is a MgO-rich olivine basalt, whereas the younger lavas of the Isleta volcano (main edifice) are predominantly alkali-enriched trachybasalts. Two of the samples from the Isleta volcano (F1 and F5) are of basaltic composition: see "Isleta Volcanoes".

TOMÉ–DALIES MAGMA RESERVOIR

Magma Source

Three lines of evidence suggest that the Tomé and Dalies volcanoes were supplied by a common magma source. First, precise $^{40}Ar/^{39}Ar$ age determinations for Tomé (3.813 ± 0.04 Ma, n = 2) and Dalies (3.83 ± 0.05 Ma, n = 3) lavas (Table 1; Dunbar et al., 2016) are analytically indistinguishable. Second, comparison of whole-rock geochemical data for Tomé and Dalies lavas (Table 4) shows a compositional similarity of major oxides and trace elements, although Tomé lavas are somewhat more mafic, as indicated by higher FeO, TiO_2, and vanadium (Table 4). Thirdly, published petrographic observations of Tomé and Dalies lavas reveal the same phenocrystic mineral assemblage of plagioclase, augite, and hypersthene (Kelly and Kudo, 1978; Dunbar et al., 2016), with basaltic hornblende occurring only in the basal lavas at Tomé Hill (Kelly and Kudo, 1978, p. 24). Tomé samples (TH-1, TH-2) collected for this study represent basal lavas that contain small, sparse phenocrysts of plagioclase plus basaltic hornblende. Samples TH-1 and TH-2 may represent a volatile-rich, crystal-poor melt near the top of the reservoir. In contrast, Dalies lavas contain a slightly higher phenocryst abundance of plagioclase and two pyroxenes, and lack hornblende (Dunbar et al., 2016), suggesting an origin from a cooler, less volatile zone in the reservoir. Taken together, these observations support the interpretation of a single magma reservoir feeding both the Tomé Hill and Dalies volcanic centers, herein referred to as the Tomé–Dalies magma reservoir (TDMR). The Tomé and Dalies volcanoes are coeval, but the eruptions are unlikely to have been contemporaneous. As mapped, the feeder dike at the Tomé Hill volcano trends east–west (090) along the hill crest and east-northeast (068) on the east flank (Kasten, 1977), and the feeder dike at the Dalies volcano trends east-southeast (Fig. 3D). These observations suggest that the Tomé–Dalies magmas ascended along a pre-rift structural grain. Ignimbrite deposits are often compositionally zoned from rhyolitic at the base to dacitic or andesitic at the top. This suggests that the more mafic Tomé Hill volcano may be slightly younger than the Dalies volcano.

Magma Volumes and Origin

The aeromagnetic expression of buried Tomé lavas extends 2.5 km west of Tomé Hill (Grauch and Connell, 2013, appendix G2). This magnetic anomaly is 2 km wide (east–west), spans 6 km from north to south, and has a linear eastern boundary trending north–south. This magnetic expression is interpreted as an originally wide lava flow, about half of which is preserved (underground) on the hanging wall of a west-down rift fault. The aeromagnetic expression of the buried Dalies lavas extends, as a 2–3-km wide belt, for 6 km to the east-southeast of the main outcrop. The original extent of Tomé and Dalies lavas is estimated at 39 km^2. Assuming an original average thickness of 50–100 m, comparable to the 280-m-high lava pile at Los Lunas (Kelly and Kudo, 1978; Love et al., 1998), implies an original eruptive volume from the TDMR of about 1.9–3.9 km^3.

Eruption of the Wind Mesa shield volcano (WMSV) predates eruption from the Tomé–Dalies reservoir by approximately 200 ka (Table 2). The WMSV is broken by a central graben, but the profile of the western block retains its shield morphology (Fig. 2). From the vent at the crest, the 4° slope descends 2 km southward over an elevation difference of 140 m. Assuming an original low-angle cone with a radius of 2 km, the exposed portion of the WMSV yields a volume of 0.6 km^3. However, the aeromagnetic expression of the WMSV (Grauch and Connell, 2013, appendix G2) shows that buried lavas extend 4 km to the north of the apical vent and 11 km southward. An original radius of 4 km for the WMSV yields a volume of ~4.67 km^3 for the shield portion. If the 5-km-wide tongue of low-gradient lava that continues 7 km to the south of the shield is about 30 m thick (~1/10 the height of the shield), that adds about 1.05 km^3 to the volume of lava erupted from the WMSV. The total volume of basaltic lava (Kelly and Kudo, 1978) erupted from WMSV is estimated to be about 5.7 km^3. Baldridge (1979) noted that none of the basaltic magmas in the Isleta area are true primitive melts from the upper mantle; all have been modified in crustal reservoirs, most likely in the lower crust. Volcanic eruptions typically extract about 20% of

TABLE 4. Summary of whole-rock XRF analyses for the Tomé Hill volcano (TH), Dalies Volcano (LLV), and Isleta volcanic complex.

Normalized Major Elements (wt%)													
Samples	SiO_2	TiO_2	Al_2O_3	FeO*	MnO	MgO	CaO	Na_2O	K_2O	P_2O_5	Ref.	°N	°W
Tomé Hill and Dalies volcanos													
TH-1	63.11	0.80	16.49	5.00	0.09	2.58	4.99	4.01	2.60	0.33	TR	34.75199	106.70403
TH-2	61.23	0.95	16.93	5.50	0.10	3.03	5.01	4.13	2.71	0.40	TR	34.75862	106.71029
LLV08	64.03	0.70	16.12	4.44	0.08	2.42	4.91	3.65	3.29	0.36	D	n.d.	n.d.
LLV11	61.83	0.86	16.35	4.98	0.09	2.75	5.34	4.18	3.04	0.58	D	n.d.	n.d.
LLV13	63.11	0.74	16.70	4.66	0.09	2.46	5.31	4.05	2.52	0.36	D	n.d.	n.d.
LLV16	63.12	0.74	16.32	4.67	0.08	2.62	5.11	4.26	2.65	0.43	D	n.d.	n.d.
Isleta volcanic complex: Isleta volcano and older river-level basalt of the Isleta Pueblo volcano													
DL-ISP-1	**49.67**	**1.90**	**15.95**	**10.78**	**0.15**	**6.47**	**10.11**	**3.30**	**1.24**	**0.42**	TR	34.90857	106.69697
DL-18	**49.75**	**2.05**	**16.05**	**10.94**	**0.17**	**6.26**	**9.41**	**3.65**	**1.25**	**0.47**	TR	34.92025	106.70607
DL-21	**50.45**	**1.67**	**15.02**	**10.99**	**0.17**	**8.27**	**8.93**	**3.29**	**0.91**	**0.30**	TR	34.91734	106.71989
F1	50.22	2.00	16.53	10.47	0.16	6.01	9.19	3.63	1.32	0.47	KK	n.d.	n.d.
DL-20	50.32	2.21	16.84	9.69	0.15	5.99	9.19	3.46	1.57	0.58	TR	34.93163	106.71553
DL-19	50.18	2.19	16.56	9.88	0.17	5.59	9.40	3.93	1.54	0.56	TR	34.91730	106.71971
F3	51.00	2.10	17.21	9.05	0.15	5.38	8.81	4.03	1.69	0.58	KK	n.d.	n.d.
114	50.62	2.15	16.65	9.68	n.d.	5.45	9.26	4.08	1.57	0.54	B	34.9191	106.7281
F5	49.71	1.87	16.86	9.95	0.15	6.30	9.83	3.66	1.23	0.44	KK	n.d.	n.d.

Trace Elements (ppm)													
	Ni	Cr	Sc	V	Ba	Rb	Sr	Zr	Y	Nb	Ga	Th	U
Tomé Hill and Dalies volcanos													
TH-1	20	26	10	91	1417	36	758	218	25	22.8	19	5	2
TH-2	29	35	10	88	1490	37	804	238	25	28.7	18	5	1
LLV08	26	44	n.d.	58	1827	36	739	234	23	22	19	5	2
LLV11	29	38	n.d.	73	1566	39	1025	240	23	34	19	10	2
LLV13	21	35	n.d.	70	1370	29	869	192	20	19	19	6	1
LLV16	28	46	n.d.	69	1686	33	922	217	22	25	19	8	2
Isleta Pueblo volcano													
DL-ISP-1	71	167	23	197	313	18	447	160	25	28.5	18	4	2

Trace Elements (ppm)						
	Cu	Zn	Pb	La	Ce	Nd
Tomé Hill and Dalies volcanos						
TH-1	24	71	12	46	80	30
TH-2	24	69	13	46	87	32
LLV08	23	66	14	n.d.	n.d.	n.d.
LLV11	25	76	14	n.d.	n.d.	n.d.
LLV13	21	68	14	n.d.	n.d.	n.d.
LLV16	25	71	14	n.d.	n.d.	n.d.
Isleta Pueblo volcano						
DL-ISP-1	58	89	4	22	48	24

n.d. = no data. Analyses of TH-1, TH-2, and DL-ISP-1 were done by Hooper Geoanalytical Laboratory. *Total iron as FeO. Analyses DL-18–DL-21 were made at the NMBGMR XRF Lab. Age data for splits of the same samples (18–21) were reported by Maldonado et al. (2007). Basalts are listed in approximate stratigraphic order, from oldest to youngest. Older MgO-rich Isleta rocks are shown with a bold font; DL-21 is a MgO-rich xenolith from Isleta Tuff. Potash-rich lavas of the Isleta volcano are shown in standard font. References (Ref.): TR, this report; KK, Kelly and Kudo (1978); B, Baldridge (1979); M, Maldonado et al. (2007); D, Dunbar et al. (2016). Alphanumeric sample numbers are the same as shown in Figures 6 and 7. Locations of samples F1, F3, and F5 (Flow 1, Flow 3, and Flow 5 of Kelly and Kudo, 1978, Table 5) are unknown. Flow F5, from near the top of the Isleta volcano, contains abundant ultramafic inclusions of wehrlite. To view sample locations using Google Earth Pro, add a hyphen ("-") before the longitude value.

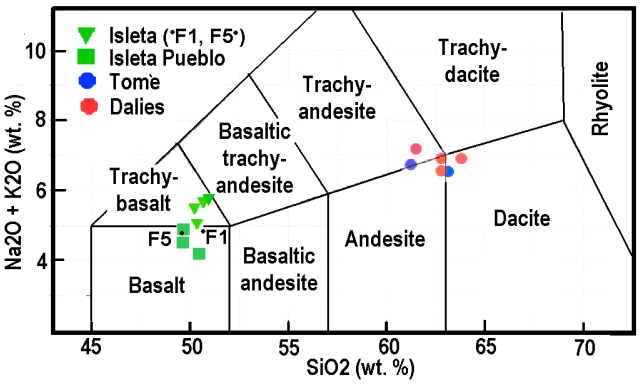


FIGURE 5. Pertinent portion of total alkali–silica (TAS) diagram showing chemical classification of samples from the Isleta volcano, Isleta Pueblo volcano, Tomé Hill volcano, and Dalies volcano. Data are from Table 4. Most of the Isleta volcano is trachybasalt and the older lava at "river level' is basalt. Basal flow of Isleta volcano (F1) is compositionally zoned (Fig. 6), with a transitional fraction of basaltic composition. Late-stage lava, flow 5 (F5), represents a third pulse of basaltic magma that forced the trachybasalt magma to the surface. Black dots indicate minor basaltic components of the Isleta volcano (see Fig. 6).

the magma from the source reservoir, leaving a little over 80% of the original magma in the crust (White et al., 2006). Thus, the original reservoir volume for the WMSV was about 29 km^3, and about 23 km^3 may have remained in the lower crustal reservoir after the eruption. The large footprint of the mid-crustal Socorro Magma Body (50 x 80 km; Balch et al., 1997) suggests that lower crustal magma reservoirs (sills) under the LLVC may have been similarly extensive.

A working hypothesis for the origin of the TDMR is as follows. After the eruption of the WMSV, a deep basaltic reservoir (lower crustal sill) of residual WMSV melt extended (or propagated) southward into the granitic crust beneath the Dalies and Tomé volcanoes. Over time, the basaltic magma percolated up along dikes into the overlying granitic crust, toward the base of a ductile mid-crustal horizon that arrested dike propagation and formed a new magma reservoir (sill). In the mid-crustal sill, the WMSV melt differentiated to basaltic andesite and assimilated a small fraction of the surrounding crust to form a hybrid mid-crustal reservoir of andesitic to dacitic magma. This assimilation and fractional crystallization model is supported by numerous granitic xenoliths in the Tomé and Dalies lavas, along with elevated $^{87}Sr/^{86}Sr$ values of 0.7057–0.7080 (Kasten, 1977).

ISLETA VOLCANOES

Age Determinations and Geochemistry

This study reports a new $^{40}Ar/^{39}Ar$ age of 2.794 ± 0.15 Ma for the "basalt island" at the Isleta Pueblo (Table 1). Although more precise, this new age is analytically indistinguishable from the mean of four duplicate ages (Table 3) published for the stratigraphically older, MgO-rich (Table 4) basaltic lavas at Isleta Pueblo (Maldonado et al., 2007; Connell et al., 2013). Duplicate ages of samples collected from the trachybasalt lavas of the Isleta volcano (Table 3; Fig. 5) also yield a mean age indistinguishable from the age of the "basalt island" at Isleta Pueblo (Table 3). Whole-rock XRF analysis (Table 4) of the "basalt island" sample (DL-ISP-1, 6.47 wt% MgO) identifies it as an MgO-rich olivine basalt chemically like another river-level lava flow sample obtained at Coors Road (DL-18, 6.26 wt% MgO). Sample DL-21 is from a large basalt block collected from the tuff breccia that directly underlies the lavas of the Isleta volcano (Isleta Tuff of Kelly and Kudo,1978). Kelly and Kudo (1978, p. 15) cite an original description of the Isleta Tuff by Herrick (1898), who states that the formation of the Isleta crater was "accompanied by explosive fragmentation of pre-existing lava whose pieces were… thrown from the crater to be lodged in the pasty mud…". Sample DL-21is an MgO-rich olivine basalt (8.27 wt% MgO) like the river-level basalt island at Isleta Pueblo. Thus Herrick's "fragments of pre-existing lava" were most likely derived from the stratigraphically older river-level basalt lava now exposed at Isleta Pueblo. In comparison, four lava samples from the main edifice of the Isleta volcano are trachybasalts (Fig. 5). Flow 1 (F1 in Figure 6; sample 1 in Kelly and Kudo, 1978) and DL-20 are interpreted to represent a compositionally zoned flow at the base of the Isleta volcano. A plot of K_2O versus MgO for all available Isleta data (Fig. 6) shows a distinct geochemical separation between river-level basalts and trachybasalt lavas of the main edifice. Lava flow 5 (F5; sample 4 in Kelly and Kudo, 1978) is near the top of the edifice. It contains abundant ultramafic inclusions of wehrlite that drive the MgO content up and K_2O down to the composition of a basalt. The temporal and geographic proximity of the Isleta Pueblo volcano and Isleta volcano implies that they were sourced from the same crustal magma reservoir. If so, the process of apparently rapid potash enrichment may have involved volatile-related redox removal of iron oxide and "alkali metasomatism" of the original tholeiitic-type basaltic melt (cf. Fig. 6 and Table 4).

A geologic map of the Isleta volcano (Kelly and Kudo, 1978, fig. 12) shows that river-level lavas are interbedded

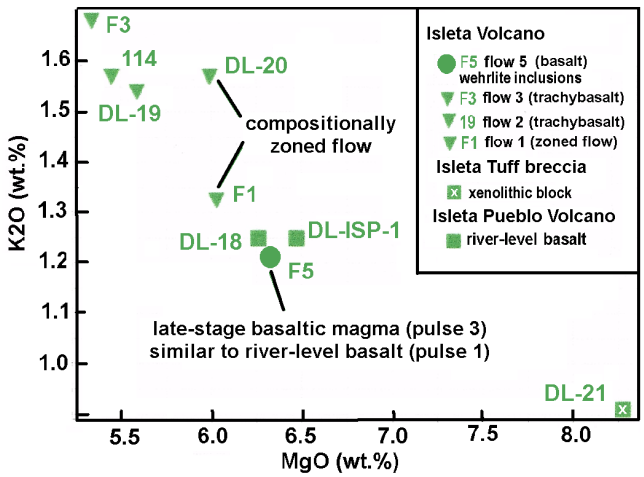


FIGURE 6. Plot of K_2O versus MgO for basaltic lavas of the Isleta volcanic complex. F1 and DL-20 are both from Flow 1 (Fig. 7), which suggests the flow is compositionally zoned. Except for sample F5, stratigraphically higher samples generally have higher K_2O content. Data are from Table 4, and sample numbers correspond to those in Table 4. Sample F5 is reported to contain abundant ultramafic wehrlite inclusions (Kelly and Kudo, 1978, p. 17).

within beds of the "Santa Fe Formation," which are now assigned to the Ceja Formation of the upper Santa Fe Group (Connell et al., 2013). Kelly and Kudo (1978) suggested that the river-level lavas below the main edifice could be correlative with the basalt at Black Mesa, newly renamed here as Rebanado Mesa (Fig. 1). However, a $^{40}Ar/^{39}Ar$ age of 2.71 ± 0.04 Ma for Rebanado Mesa (Table 2) now indicates that it is distinctly younger than the precise age of 2.794 ± 0.015 Ma for the "basalt island" lava. Figure 7 illustrates an interpretation of the stratigraphic relationship between the river-level basalts (basalt of the Isleta Pueblo volcano); the pyroclastic breccia, which contains large basaltic blocks (black squares in Fig. 7); and the overlying trachybasalts of the main edifice. Considering the likelihood of explosive scouring related to the formation of the tuff breccia, the river-level basalt (heavy black line in Fig. 7) may have been buried by about 7–10 m of Ceja Formation beds before the pyroclastic eruption, which was followed by lavas of the main edifice. Given analytical uncertainties (Table 3), the Isleta volcano could be as much as 40–60 ka younger than the river-level basalt of the Isleta Pueblo volcano.

Petrographic observation of the "basalt island" sample (DL-ISP-1) shows about 7% euhedral olivine phenocrysts, but clinopyroxene occurs only as a groundmass mineral. This implies that the river-level lava erupted at a temperature above the clinopyroxene liquidus, at ~1,160°C. Coarser crystalline plagioclase and clinopyroxene occur only in glomerophyric aggregates, which suggests that the high-temperature tholeiitic magma had intruded and disrupted a slowly cooled, preexisting gabbro or gabbroic mush. The presence of sparse clinopyroxene phenocrysts in the main edifice lavas (Kelly and Kudo, 1978, p. 17) therefore supports the interpretation that the reservoir melt had cooled down somewhat and become enriched in potash. One important observation of Kelly and Kudo is that the uppermost lavas (F5, Fig. 7) contain ultramafic inclusions of wehrlite. As noted earlier, these are apparently abundant enough to drive the MgO content back into the olivine basalt class (F5, Fig. 6). Together, these observations are consistent with the interpretation that the Isleta volcanic complex records the effects of incremental melt additions to a lower crustal basaltic magma reservoir. Initial eruption of a tholeiitic-type magma from a crustal reservoir was followed shortly thereafter by eruption of a slightly cooled residual magma, enriched in potash. The second eruption was presumably driven by a newly added increment of tholeiitic magma that disrupted some mafic crystal layers at the bottom of the reservoir and re-energized the preexisting reservoir.

DISCUSSION

Precise $^{40}Ar/^{39}Ar$ age determinations are a key to understanding the magmatic and eruptive evolution of the Los Lunas volcanic cluster. Precise ages allow recognition of the relative timing and sequence in a chain of volcanic events. The timing, sequence, volume, and composition of volcanic events in a coeval cluster essentially provide a recipe for open-system magma mixing, differentiation, and assimilation in the underlying crust. New and published age data (Table 2) demonstrate that the eroded remnants of the ~3.8-My-old Tomé Hill and Dalies volcanoes are virtually the same age (±50 ka) and are of similar composition (Table 4) and equivalent mineralogy (Kasten, 1977; Dunbar et al., 2016); yet they are 10 km apart (Fig. 1). This unexpected discovery makes sense only when placed into the context of a larger magma reservoir system, of which the Los Lunas volcanic cluster (LLVC) is an expression. The inferred singular Tomé–Dalies magma reservoir (TDMR) is apparently not unique. Magnetotelluric data imply that the Mount St. Helens and Mount Adams volcanoes, of the Cascadian arc, are linked by a singular mid-crustal conductive zone, which is interpreted as a mid-crustal magma or magma mush reservoir that links the active volcanoes (Hill et al., 2009)

The cluster of nine late Cenozoic basaltic centers near Isleta is probably not the expression of a "mini hot spot" in the upper mantle, as there is no indication that it has migrated eastward over the past 4 million years. Observed high seismic velocities under the northern LLVC imply that the cluster of basaltic volcanoes at Wind Mesa, Isleta, and Cat Hills lies at the top of a relatively small block (15 x 20 x 40 km) of mafic crystalline

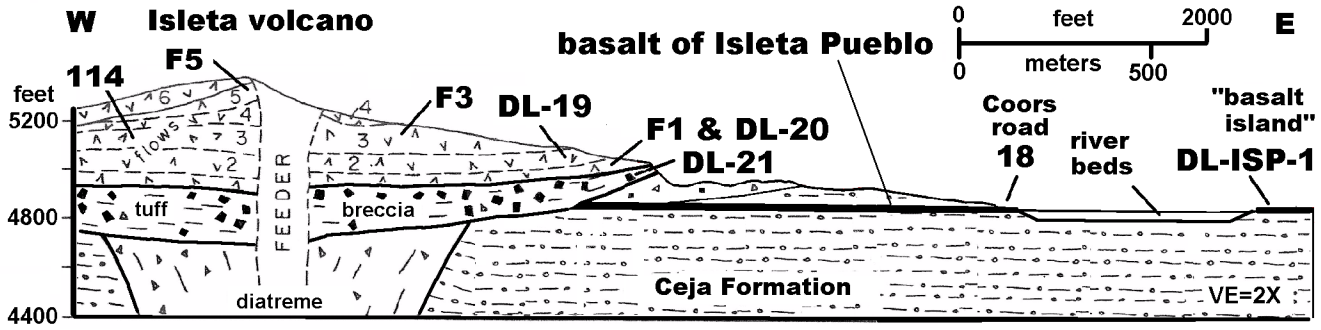


FIGURE 7. Cross-section (modified after Kelly and Kudo, 1978, fig. 16) illustrating the stratigraphic relationship between the "basalt of Isleta Pueblo," also called the "basalt island," and trachybasalt lavas (flows labeled 1–6) of the main edifice at the Isleta volcano. Ballistic blocks (sample DL-21) explosively derived from the older basalt of Isleta Pueblo are illustrated as black rectangles in the tuff breccia (Isleta Tuff) that underlies the Isleta volcano. Open triangles represent juvenile pumice or scoria. Sample locations are projected to the line of section. Locations of three samples collected by Kelly and Kudo (1978) were mistakenly not shown on their figure 12, but are referenced in Figure 7 here using the following labels: F1 (their sample 1), F3 (their sample 3), and F5 = (their sample 4). These and other samples (114, DL-19, DL-20, DL-21, DL-18, DL-ISP-1) correspond to those in Table 4 and Figure 6.

basement at about 3–40 km depth, corresponding to previously mapped high-velocity crust (Golos et al., 2020). This inferred transcrustal gabbroic block is here proposed to act as a preferential and refractory "magma pipeline" suitable for transporting high-temperature basaltic magmas from lower crustal sills to the surface via magma-driven hydraulic fractures equivalent to dikes. For future reference, this hypothetical "refractory-magma conduit" for basaltic magmas could be given the label "MaMagPi," for mafic magma pipeline. A large basaltic lava field of mostly Pleistocene age in western Oregon, the Boring volcanic field (BVF), is built upon a large fragment of imbedded oceanic crust known as the Accreted Siletzia terrane and is considered to represent "anomalous forearc magmatism" (Leeman, 2020). Leeman states that the close association of the Boring volcanic field with the oceanic Siletzia terrane "may not be coincidental." The gabbroic oceanic crust of the Siletzia terrane may be analogous to the much smaller velocity anomaly under the cluster of basaltic volcanoes at Isleta. The BVF may be a generally misunderstood example of the effect of a MaMagPi.

The origin of the high-seismic-velocity anomaly under Isleta is generally beyond the scope of this discussion. However, the most likely candidate is a down-dropped fragment of the Tijeras greenstone belt (TGB), which underlies the Manzanita Mountains east of Isleta (Condie, 1980). The inferred higher density of the gabbroic and basaltic TGB (~2.8–3.0 Mt/m^3) has muted the isostatic rebound of the Manzanita Mountains, compared to the much higher Sandia Mountains and Manzano Mountains that are underlain by lower density granitic rocks (Condie and Budding, 1979).

Volcanic eruptions often become focused with time. Closely spaced and overlapping eruptions at Isleta, Los Lunas, and the Cat Hills are examples. The Isleta complex (Isleta and Isleta Pueblo volcanoes) clearly represents pulsed eruptions indicative of incremental magma intrusions at depth. The first eruption was more fluid and at higher temperature, whereas the delayed second eruption was more volatile and explosive. A subtle third magma pulse may have forced the second eruption.

CONCLUSIONS

New age determinations for Tomé Hill volcano and the "basalt island" at Isleta Pueblo, when coupled with published age and geophysical data, provide new insights into rift-related volcanism and magmatism in the central Albuquerque Basin. These insights, or conclusions, are:

1. The cluster of nine late Cenozoic basaltic volcanoes around Isleta probably represents the surface expression and effect of underlying high-seismic-velocity mafic crust (e.g., gabbro) favorable for transporting high-temperature basaltic melt rapidly to the surface via melt-driven hydraulic fractures (dikes).
2. At what is now Isleta Pueblo, a high-temperature basalt eruption at about 2.81 Ma was followed shortly thereafter (<40 ka) by a more volatile and explosive eruption of potassic trachybasalt magma. The second eruption was likely driven by a third magma pulse of basaltic composition, quite like the first pulse.
3. Basaltic magma that remained in the crust after eruption of the relatively large volume Wind Mesa shield volcano was likely the initial melt supply that then formed coeval hybrid dacite eruptions at Tomé Hill and Dalies volcanoes.
4. Volcanism at one center often occurs as pulses (decades to millennia apart) yielding precise $^{40}Ar/^{39}Ar$ ages that are indistinguishable; so stratigraphic and compositional differences can be crucial data for resolving the order of eruptions.
5. Volcanism and magmatism in the Albuquerque Basin is probably underrated because the late Cenozoic volcanoes are rapidly buried by basin-fill deposits in the subsiding rift.

ACKNOWLEDGMENTS

Mike Timmons, director of the New Mexico Bureau of Geology and Mineral Resources, is thanked for the logistical support of emeritus staff and the encouragement of all Bureau staff in their research on New Mexico geology. DL thanks John Sorrell (Isleta Pueblo geohydrologist) and Mike Marshall for their help with mapping and obtaining samples from Isleta. Many thanks to Zohreh Kazemi Motlagh, who assisted in the construction of Figures 5 and 6. RC also owes his wife Louise a huge thank you for helping him beat cancer and then letting him work overtime—in retirement. Reviews by Jayne Aubele and Nels Iverson provided many helpful suggestions that improved the clarity of the manuscript.

Edits by Rebecca Barr and Dan Koning provided a more concise and consistent final copy of the manuscript.

REFERENCES

Annen, C., 2011, Implications of incremental emplacement of magma bodies for magma differentiation, thermal aureole dimensions, and plutonism volcanism relationships: Tectonophysics, v. 500, no. 1–4, p. 3–10. https://doi.org/10.1016/j.tecto.2009.04.010

Bachman, G.O., and Mehnert, H.H., 1978, New K-Ar dates and the late Pliocene to Holocene geomorphic history of the central Rio Grande region, New Mexico: Geological Society of America Bulletin, v. 89, p. 283–292. https://doi.org/10.1130/0016-7606(1978)89<283:NKDATL>2.0.CO;2

Balch, R.S., Hartse, H. E., Sanford, A.R., and Lin, K., 1997, A new map of the geographic extent of the Socorro Mid-Crustal magma body: Bulletin of the Seismological Society of America, v. 87, no. 1, pp. 174–182. https://doi.org/10.1785/BSSA0870010174

Baldridge, W.S., 1979, Petrology and petrogenesis of Plio-Pleistocene basaltic rocks from the central Rio Grande rift, and their relation to rift structure, *in* Riecker, R.E., ed., Rio Grande Rift: Tectonics and Magmatism: Washington, D.C., American Geophysical Union, p. 323–353. https://doi.org/10.1029/SP014p0323

Buck, W.R., 2004, Consequences of asthenospheric variability on continental rifting, *in* Karner, G.D., Taylor, B., Driscol, N.W., and Kohlstedt, D.L., eds., Rheology and Deformation of the Lithosphere at Continental Margins: New York, Columbia University Press, p. 1–30. https://doi.org/10.7312/karn12738-002

Cashman, K.V., Sparks, R.S.J., and Blundy, J.D., 2017, Vertically extensive and unstable magmatic systems: A unified view of igneous processes: Science 355, eaag3055. https://doi.org/10.1126/science.aag3055

Chamberlin, R.M., McIntosh, W.C., and Eggleston, T.L., 2004, $^{40}Ar/^{39}Ar$ geochronology and eruptive history of the eastern sector of the Oligocene Socorro caldera, central Rio Grande rift: New Mexico: Bureau of Geology and Mineral Resources, Bulletin 160, p. 251–279.

Condie, K.C., 1980, The Tijeras greenstone: Evidence for depleted upper mantle beneath New Mexico during the Proterozoic: Journal of Geology, v. 88, p. 603–609. https://doi.org/10.1086/628546

Condie, K.C., and Budding, A.J., 1979, Geology and geochemistry of Precambrian rocks, central and south-central New Mexico: New Mexico Bureau of Mines and Mineral Resources, Memoir 35, 58 p. https://doi.org/10.58799/M-35

Connell, S.D., 2004, Geology of the Albuquerque Basin and tectonic development of the Rio Grande rift in north-central New Mexico, *in* Mack, G.H., and Giles, K.A., eds., The Geology of New Mexico: A Geologic History: Socorro, New Mexico Geological Society, p. 359–388.

Connell, S.D., 2008, Refinements to the stratigraphic nomenclature of the Santa Fe Group, northwestern Albuquerque Basin, New Mexico, New Mexico Geology, v. 30, no. 1, p. 14–35. https://doi.org/10.58799/NMG-v30n1.14

Connell, S.D., Love, D.W., Sorrel, J.D., and Harrison, J.B.J., 2001, Plio-Pleistocene stratigraphy and geomorphology of the central part of the Albuquerque Basin (Friends of the Pleistocene Meeting, Oct 12-14, 2001): New Mexico Bureau of Geology and Mineral Resources, Open-file report 454C-D, p. 1-1–1-28, 2-1–2-23, 3-1–3-13.

Connell, S.D., Smith, G.A., Geissman, J.W., and McIntosh, W. C., 2013, Climatic controls on nonmarine depositional sequences in the Albuquerque Basin, Rio Grande rift, north-central New Mexico, *in* Hudson, M.R., and Grauch, V.J.S., eds., New Perspectives on Rio Grande Rift Basins: From Tectonics to Groundwater: Geological Society of America, Special Paper 494, p. 383–425. https://doi:10.1130/2013.2494(15)

Debayle, E., Bodin, T., Durand, S., and Yanick, R., 2020, Seismic evidence for partial melt below tectonic plates: Nature, v. 586, p. 555–559. https//doi.org/10.1038/s41586-020-2809-4

Dunbar, N.W., McIntosh, W.C., Love, D.W., Panter, K.S., and Hallett, B., 2016, Two eruptive episodes of Los Lunas Volcano: Geochemistry and $^{40}Ar/^{39}Ar$ age determination using electron microprobe sample evaluation: New Mexico Geological Society, Guidebook 67, p. 203–216. https://doi.org/10.56577/FFC-.203

Golos, E.M., Fang, H., and van der Hilst, R.D., 2020, Variations in seismic wave speed and *Vp*/*Vs* ratio in the North American lithosphere: Journal of Geophysical Research Solid Earth, v. 125, E2020 JB 020574. https://doi.org/10.1029/2020JB020574

Grauch, V.J.S., and Connell, S.D., 2013, New perspectives on the geometry of the Albuquerque Basin, Rio Grande rift, New Mexico: Insights from Geophysical Models of rift-fill thickness, *in* Hudson, M. R., and Grauch, V.J.S., eds., New Perspectives on Rio Grande Rift Basins: From Tectonics to Groundwater: Geological Society of America, Special Paper 494, p. 427–462. https: doi:10.1130/2013.2494(16)

Herrick, C.L., 1898, Geology of the environs of Albuquerque, New Mexico: American Geologist, v. 22, p. 26–43.

Hill, G., Caldwell, T., Heise, W., Chertkoff, D., Bibby, H., Burgess, M., Cull, J., and Cas, A., 2009, Distribution of melt beneath Mount St Helens and Mount Adams inferred from magnetotelluric data: Nature Geoscience, v. 2, p. 785–789. https://doi.org/10.1038/ngeo661

Kasten, J.A., 1977, Petrology and geochemistry of calc alkaline andesites within the Albuquerque Basin, Valencia County, New Mexico [M.S. thesis]: Albuquerque, University of New Mexico, 79 p.

Katz, R.F., Spiegelman, M., and Holtzman, B., 2006, The dynamics of melt and shear localization in partially molten aggregates: Nature, v. 442, p. 676–679. https://doi.org/10.1038/nature05039

Kelley, V.C., and Kudo, A.M., 1978, Volcanoes and related basalts of Albuquerque Basin, New Mexico: New Mexico Bureau of Geology and Mineral Resources, Circular 156, 30 p. https://doi.org/10.58799/M-33

Kuiper, K. F., Deino A., Hilgen, F. J., Krijgsman, W., Renne, P. R., and Wijbrans, J. R., 2008, Synchronizing the rock clocks of Earth history: Science, v. 320, p. 500–504. https://doi.org/10.1126/science.1154339

Leeman, W.P., 2020, Old/new subduction zone paradigms as seen from the Cascades: Frontiers of Earth Science, v. 8, 535879. https://doi.org/10.3389/feart.2020.535879

Love, D.W., Maldonado, F., Hallett, B., Panter, K., Reynolds, C., McIntosh, W.C., and Dunbar, N., 1998, Geology of the Dalies 7.5-minute quadrangle: New Mexico Bureau of Geology and Mineral Resources, Open-file Geologic Map OF-GM-21, scale 1:24,000.

Love, D.W., McIntosh, W.C., Dunbar, N., and Connell, S.D., 2001, Third day road log: Geology of Los Lunas volcano: New Mexico Bureau of Geology and Mineral Resources, Open-file Report 454C-D, 13 p.

Mahon, K.I., 1996, The New "York" regression: Application of an improved statistical method to geochemistry: International Geology Review, v. 38, p. 293–303. https://doi.org/10.1080/00206819709465336

Maldonado, F., Slate, J.L., Love, D.W., Connell, S.D., Cole, J.C., and Karlstrom, K.E., 2007, Geologic map of the Pueblo of Isleta tribal lands and vicinity, Bernalillo, Torrance, and Valencia Counties, central New Mexico: U.S. Geological Survey Scientific, Investigations Map 2913, scale 1:50,000, 35 p. https://doi.org/10.3133/sim2913

McDougall, I., and Harrison, T.M., 1999, Geochronology and thermochronology by the $^{40}Ar/^{39}Ar$ Method: New York, Oxford University Press, 269 p.

Min, K., Mundil, R., Renne, P.R., and Ludwig, K.R., 2000, A test for systematic errors in $^{40}Ar/^{39}Ar$ geochronology through comparison with U–Pb analysis of a 1.1 Ga rhyolite: Geochimica et Cosmochimica Acta, v. 64, p. 73–98. https://doi.org/10.1016/S0016-7037(99)00204-5

Nier, A.O., 1950, A redetermination of the relative abundances of the isotopes of carbon, nitrogen, oxygen, argon, and potassium: Physical Review, v. 77, p. 789–793. https://doi.org/10.1103/PhysRev.77.789

Ross, J., 2019, NMGRL/pychron, version 18.2: Zenodo.

White, S.M., Crisp, J.A., and Spera, F J., 2006, Long term volumetric eruption rates and magma budgets: Geochemistry Geophysics Geosystems, v. 7, Q03010. https://doi:10.1029/2005GC001002

Zimmerer, M.J., 2024, A temporal dissection of late Quaternary volcanism and related hazards within the Rio Grande Rift and along the Jemez lineament of New Mexico, USA: Geosphere, v.20, no. 2, p. 505–546. https://doi.org/10113/GES02576.1

Appendices can be found at
https://nmgs.nmt.edu/repository/index.cfml?rid=2026003



Fallen block of basalt along the Boca Negra trail showing several petroglyphs, including a bird and both male and female figures. A vesicle cylinder emanates from the left hand (or claw?) of the right figure. Although not explicit here, occasionally Ancestral Puebloan artists incorporated vesicle cylinders into their art at the Albuquerque Volcanoes (see Goff, this volume). Photograph courtesy of Fraser Goff.